

Functional characterization of a VEGF-A-targeting Anticalin, prototype of a novel therapeutic human protein class

Hendrik Gille^{1,4} · Martin Hülsmeier¹ · Stefan Trentmann¹ · Gabriele Matschiner¹ · Hans Jürgen Christian¹ · Todd Meyer³ · Ali Amirkhosravi³ · Laurent P. Audoly¹ · Andreas M. Hohlbaum¹ · Arne Skerra²

Received: 9 March 2015 / Accepted: 1 November 2015
© Springer Science+Business Media Dordrecht 2015

Abstract Human tear lipocalin (Tlc) was utilized as a protein scaffold to engineer an Anticalin that specifically binds and functionally blocks vascular endothelial growth factor A (VEGF-A), a pivotal inducer of physiological angiogenesis that also plays a crucial role in several neovascular diseases. Starting from a naive combinatorial library where residues that form the natural ligand-binding site of Tlc were randomized, followed by affinity maturation, the final Anticalin PRS-050 was selected to bind all major splice forms of VEGF-A with picomolar affinity. Moreover, this Anticalin cross-reacts with the murine ortholog. PRS-050 efficiently antagonizes the interaction between VEGF-A and its cellular receptors, and it inhibits VEGF-induced mitogenic signaling as well as proliferation of primary human endothelial cells with subnanomolar IC₅₀ values. Intravitreal administration of the Anticalin suppressed VEGF-induced blood–retinal barrier breakdown in a rabbit model. To allow lasting systemic neutralization of VEGF-A in vivo, the plasma half-life of the Anticalin was extended by site-directed PEGylation. The modified Anticalin efficiently blocked VEGF-mediated

vascular permeability as well as growth of tumor xenografts in nude mice, concomitantly with reduction in microvessel density. In contrast to bevacizumab, the Anticalin did not trigger platelet aggregation and thrombosis in human FcγRIIIa transgenic mice, thus suggesting an improved safety profile. Since neutralization of VEGF-A activity is well known to exert beneficial effects in cancer and other neovascular diseases, including wet age-related macular degeneration, this Anticalin offers a novel potent small protein antagonist for differentiated therapeutic intervention in oncology and ophthalmology.

Keywords Angiogenesis · Cancer · Lipocalin · Protein engineering · Protein scaffold

Introduction

The broad potential of monoclonal antibodies as reagents for molecular recognition, especially for medical applications, has been validated during the past decade through their remarkable therapeutic and commercial success [1, 2]. Nevertheless, due to several practical limitations, such as large molecular size, complex composition, posttranslational modification, and sometimes undesired immunological effector functions, different alternative protein scaffolds, in particular lipocalins, have been proposed as novel binding reagents and were successfully engineered for specific target recognition [3, 4].

Lipocalins comprise a class of functionally diverse proteins [5] that are found in most phyla of life and serve for the transport, storage or sequestration of endogenous or exogenous small molecules. They are secretory proteins, usually monomeric with 150–180 residues, and mostly occur in the body fluids, including blood as well as

✉ Gabriele Matschiner
Matschiner@pieris.com

✉ Arne Skerra
skerra@tum.de

¹ Pieris Pharmaceuticals GmbH, Lise-Meitner-Strasse 30, 85354 Freising, Germany

² Lehrstuhl für Biologische Chemie, Technische Universität München, 85350 Freising-Weihenstephan, Germany

³ Center for Thrombosis Research, Florida Hospital, Orlando, FL, USA

⁴ Present Address: Silence Therapeutics GmbH, Robert-Rössle-Str. 10, 13125 Berlin, Germany

exocrine and endocrine secretions. Despite very low mutual sequence homology, lipocalins share a common fold with a conserved eight-stranded antiparallel β -barrel and an α -helix attached to its side [6, 7]. At one end, the β -barrel is closed by short loops and densely packed side chains, whereas the other end is open to solvent. There, four loops connect neighboring β -strands in a pairwise fashion and form the entrance to the natural ligand pocket. These loops are hypervariable in terms of conformation, length and sequence, which reflects the variety of observed binding specificities for vitamins, hormones and secondary metabolites, or even catalytic function in some cases.

More than 15 different lipocalins are currently known in humans [7]. The plasma retinol-binding protein (RBP), which transports the chemically sensitive and poorly soluble vitamin A from the liver via the blood stream to several tissues, is the prototypic member of this family, whose three-dimensional structure was solved first [8]. Other human lipocalins, such as the neutrophil gelatinase-associated lipocalin (NGAL) [9] and also tear lipocalin (Tlc) [10], play a role in innate immunity by scavenging siderophores and thus inhibiting microbial growth [11]. Following initial studies wherein the binding pocket of an insect lipocalin was successfully reshaped to recognize hapten-like molecules such as fluorescein [12], we have also described the engineering of human NGAL to specifically recognize protein ‘antigens’ of biomedical relevance with subnanomolar affinity, for example CTLA-4 [13] and the fibronectin extradomain B [14].

In contrast to NGAL, Tlc shows a pronounced ligand promiscuity [15], indicating enhanced flexibility of its binding site [16, 17]. Hence, Tlc provides another promising scaffold for the engineering of lipocalins with novel specificities, so-called Anticalins. We have recently described the properties of a Tlc-derived Anticalin targeting the extracellular domain of the c-met receptor [18]. In the present study, we report on vascular endothelial growth factor A (VEGF-A), an important signaling molecule for the formation of new blood vessels [19], as target of an Anticalin with neutralizing properties and therapeutic potential.

While VEGF-A exerts physiological functions during developmental growth as well as wound healing and the female reproductive cycle in the adult, significant scientific interest has focused on its role in pathological angiogenesis. In fact, it was demonstrated that VEGF-A inhibition by an antagonistic monoclonal antibody led to significantly reduced angiogenesis and tumor growth in several xenograft models [20]. Since then the therapeutic success of the biologics bevacizumab, ranibizumab and aflibercept has confirmed the central role of this growth factor in pathological angiogenesis, especially in oncology [21].

However, while bevacizumab (Avastin), a humanized VEGF-A-neutralizing antibody, is usually well tolerated,

significant toxicities occur in a subset of patients, for example gastrointestinal perforations and thromboembolic events [22–24]. Indeed, it has been demonstrated that bevacizumab can form multimeric immune complexes with its inherently dimeric antigen *in vivo*, which may cause some of these effects [25]. Furthermore, immune complex deposition in the kidney can lead to glomerulosclerosis [26]. Thromboembolic complications of bevacizumab can be mimicked in human Fc γ receptor IIa (Fc γ RIIa) transgenic mice, where administration of complexes between heparin, bevacizumab and heparin-binding isoforms of VEGF-A evoke platelet aggregation and thrombosis [27].

Here, we describe a VEGF-A-specific Anticalin that differs from all other previously developed VEGF antagonists by its unique monomeric structure and safety profile, including absence of adverse effects on platelets in Fc γ RIIa transgenic mice, thus offering an alternative biological reagent with therapeutic potential.

Results

Engineering and initial characterization of an Anticalin specific for VEGF-A

A recombinant core fragment of VEGF-A lacking the heparin-binding domain (VEGF_{8–109}) was produced in *E. coli* by refolding from inclusion bodies to yield the soluble homodimeric protein [28] and used as target for phage display selection and ELISA screening of cognate Anticalin candidates. A random library of human Tlc with high combinatorial complexity was prepared by concerted mutagenesis of multiple amino acid positions in the four loops of the mature recombinant wild-type protein [16]. To this end, a gene cassette wherein the corresponding codons were randomized in a targeted fashion was assembled via polymerase chain reaction (PCR) with degenerate primer oligodeoxynucleotides according to a previously described strategy [29].

From this Anticalin library, an initial lead candidate was isolated by phagemid display in combination with ELISA screening via small-scale *E. coli* expression of the soluble lipocalin variants. This candidate exhibited antagonistic properties with respect to the interaction between full-length VEGF-A (VEGF₁₆₅) and the extracellular region of VEGFR-2 in an ELISA and also cross-reactivity with the murine VEGF ortholog. In the course of several affinity maturation steps by applying partial mutagenesis of the lipocalin coding region and phagemid panning as well as ELISA screening under more stringent conditions, the target affinity of the Anticalin candidate was improved from $K_D = 400$ nM to 25 pM.

The final Anticalin, PRS-050, was expressed as a soluble protein via periplasmic secretion in *E. coli* and purified to homogeneity. The thermal stability of this engineered lipocalin was assessed by circular dichroism (CD) measurements, revealing a remarkably high melting temperature of 75 °C. The Anticalin was further characterized with regard to recognition of different human VEGF-A splice forms as well as rodent orthologs. In line with the high degree of sequence conservation between human and murine VEGF-A (90 % amino acid identity), comparable high-affinity binding was detected in surface plasmon resonance (Biacore) measurements using the Anticalin immobilized on the chip surface. This contrasts with bevacizumab, which recognizes an epitope that is unique to human VEGF-A [22].

Likewise, PRS-050 exhibited picomolar binding activities for all human VEGF-A splice forms. The most abundant versions, human VEGF₁₆₅ as well as rat VEGF₁₆₄, showed virtually identical affinities of 25 and 21 pM, respectively. Importantly, the selected Anticalin did not bind any of the more distantly related human vascular growth factors, i.e., VEGF-B, VEGF-C, VEGF-D and PLGF, with detectable affinity. Thus, combinatorial engineering of Tlc has led to a stable novel binding protein with favorable specificity and high target affinity.

Assessment of in vitro affinity and biological efficacy

The ability of the Tlc-based Anticalin to interfere with VEGF-A-induced mitogenic signaling and proliferation was investigated in comparison with the well-known antibody bevacizumab using primary human umbilical vein endothelial cells (HUVECs). Stimulation of HUVECs with VEGF-A, via binding to VEGFR-2, leads to dual phosphorylation and activation of extracellular signal-regulated kinases (ERKs) 1 and 2 [30]. HUVECs were treated with VEGF-A (20 ng/mL VEGF₁₆₅) in the presence of either antagonist, and phosphorylated ERK1/2 was quantified in a whole-cell ELISA after fixation and permeabilization. Both the Anticalin and bevacizumab inhibited VEGF-induced ERK phosphorylation with similar potency. In fact, PRS-050 revealed an even lower IC₅₀ value of 4.5 nM versus 13 nM for the bivalent antibody (Fig. 1a).

To further compare the in vitro efficacy of these two protein reagents, we assessed their ability to interfere with VEGF-mediated HUVEC proliferation. Again, the Anticalin and bevacizumab exhibited similar antagonistic activities (Fig. 1b). The effect was specific for VEGF-A since signaling and proliferation mediated by FGF-2 (basic fibroblast growth factor, b-FGF) were not influenced by either the Anticalin or bevacizumab. These data demonstrate potent in vitro inhibition of VEGF-A activity on endothelial cells by the Anticalin.

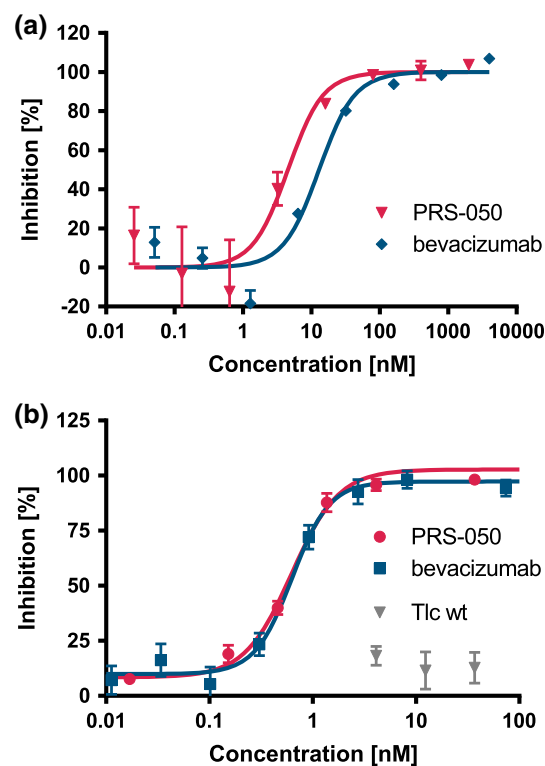


Fig. 1 Anticalin PRS-050 inhibits mitogenic signaling in HUVECs. **a** Phosphorylation of ERK1 and ERK2 was assessed by cell ELISA following VEGF-A (20 ng/mL) stimulation of cells in the presence of the indicated antagonist concentrations (molarity of the antibody was calculated assuming a molecular mass of 150 kDa). **b** Cells were stimulated with VEGF-A (20 ng/mL) over a period of 5 days in the presence of antagonists; subsequently, viability was assessed by luminescence-based quantification of intracellular ATP

Inhibition of rabbit blood/retinal barrier breakdown

Intravitreal injection of recombinant human VEGF-A into the rabbit eye leads to a breakdown of the blood–retinal barrier (BRB), characterized by leaky retinal vessels and retinal leukocyte stasis [31, 32], which can be blocked by administration of a VEGF-A-neutralizing antibody [31]. In order to compare the activity of PRS-050 with that of the clinically approved anti-VEGF Fab fragment ranibizumab (Lucentis) [33] in this model we first investigated its half-life in the rabbit eye following intravitreal injection. Pharmacokinetic (PK) analysis resulted in a terminal half-life of 2.9 days for the Anticalin in the vitreous (Fig. 2a), which is in the same range as the half-life reported for ranibizumab in this compartment [34].

The VEGF-A blocking effect was investigated by first injecting the right eye of a rabbit with either the Anticalin, recombinant wild-type (wt) Tlc or ranibizumab. After 5 days, human VEGF-A was additionally injected into the vitreous of the right eye. Further 2 days later, animals received an intravenous injection of fluorescein, and

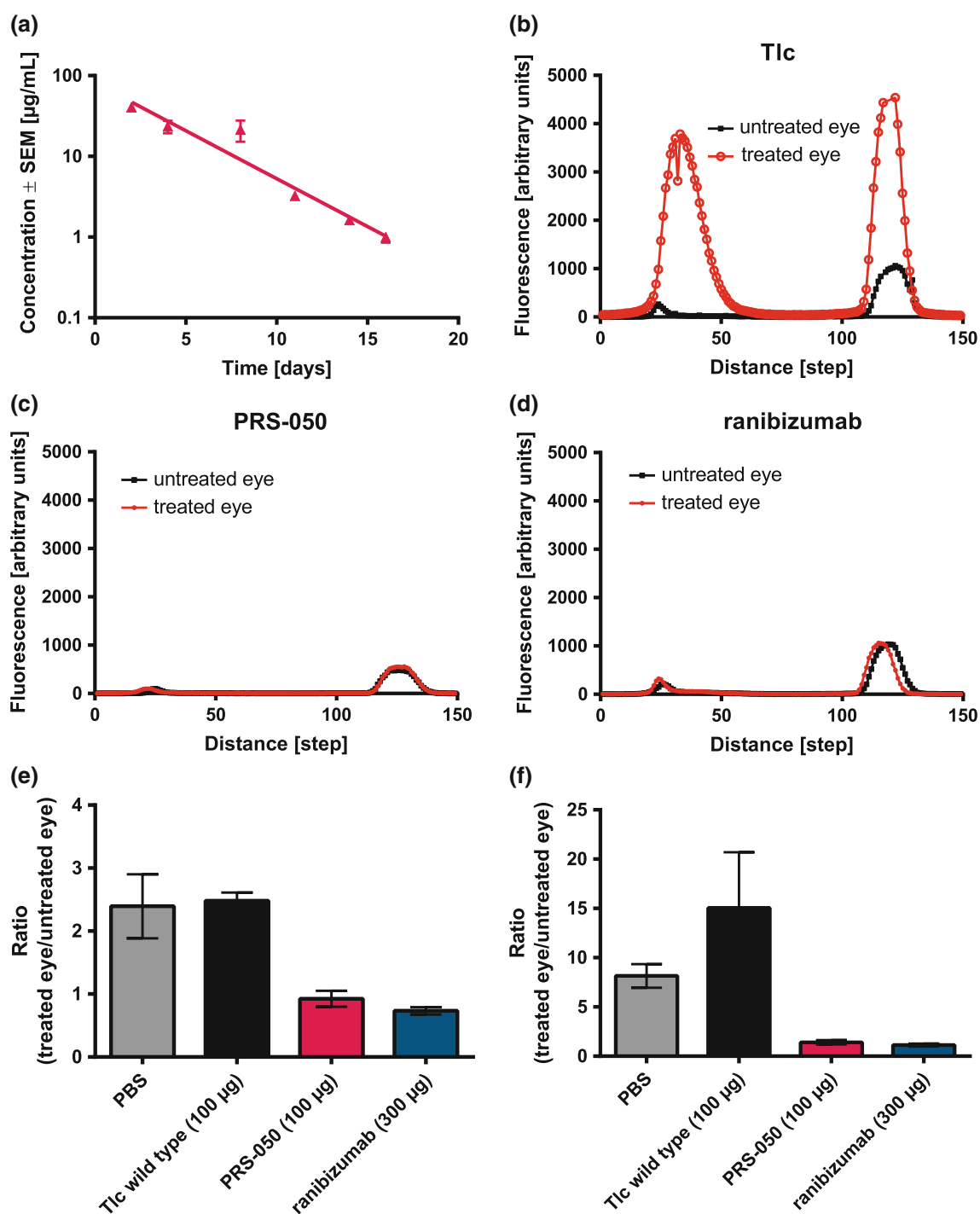


Fig. 2 PRS-050 pharmacokinetics and VEGF-A blocking activity in the rabbit eye. **a** Anticalin concentrations in the vitreal fluid following intravitreal injection were determined by sandwich ELISA over a period of 16 days ($n = 4$ eyes per time point). **b–d** The extent of breakdown of the blood–retinal barrier after intravitreal injection of rhVEGF₁₆₅ (500 ng) was assessed by fluorophotometry following intravenous fluorescein injection. The distance from the cornea on the optical axis toward the retina is shown (in 148 steps). Representative scans for one animal from each group treated with either wtTlc

(100 μg), PRS-050 (100 μg), or ranibizumab (100 μg) are depicted. The *left peaks* represent the posterior (vitreous and retina) fluorescence, whereas the *right peaks* correspond to anterior chamber fluorescence. The *untreated (left)* eye received neither VEGF-A nor the test antagonist protein. **e** Mean ratios of fluorescence between treated and untreated eyes of each group are depicted for anterior segment (cornea and anterior chamber). **f** Mean ratios of fluorescence between treated and untreated eyes of each group are depicted for the posterior segment (vitreous and retina)

leakage into the anterior and posterior segments of both the treated and the contralateral control eye was quantified using noninvasive scanning ocular fluorophotometry. Examples of representative scans from each of the three groups are depicted (Fig. 2b–d). Mean area under the curve (AUC) values for the anterior and posterior segments were calculated from all scans (Fig. 2e, f). As result, a single intravitreal injection of the Anticalin clearly inhibited VEGF-induced BRB breakdown, whereas injection of wtTlc did not have a significant effect. Functional neutralization of VEGF was almost complete in case of the Anticalin pre-treatment and similar to an equimolar dose of ranibizumab, indicating comparable activity in this model.

Plasma half-life extension of PRS-050

Due to their small molecular size of around 20 kDa, rapid excretion via the kidney is the major elimination pathway of Anticalins from circulation, resulting in relatively short half-lives compared to antibodies. To prolong the *in vivo* half-life of the Anticalin for systemic applications, a free cysteine residue was introduced at the β -barrel surface of the lipocalin scaffold, remote from the loop region, thus allowing site-specific PEGylation [35]. Following expression and purification of the modified protein in *E. coli*, this residue was used for coupling with 20 kDa, 30 kDa, and branched 40 kDa PEG-maleimide. The biochemical homogeneity of the purified conjugates was confirmed by SDS-PAGE (Fig. 3a).

The plasma PK parameters of these PEGylated Anticalin versions were determined after bolus *i.v.* administration in mice (Table 1; Fig. 3b). Non-compartmental PK analysis indicated that PEGylation resulted in a significant extension of the terminal half-life from below 1 h for the unmodified Anticalin (not shown) to 28 h for the 40 kDa PEGylated version. The Anticalin carrying a 40 kDa branched PEG moiety was selected for further investigation in order to maximize drug exposure *in vivo*.

To investigate VEGF-A binding activity of the 40 kDa PEGylated Anticalin, surface plasmon resonance (SPR) measurements were made in direct comparison with the unmodified protein. While the affinity of the PEGylated form was still subnanomolar, its K_D value was increased by a factor of 5. This effect was due to a slower on-rate after PEGylation as the off-rates of both versions were essentially the same (Table 2). A lowered on-rate of binding following PEGylation is consistent with observations reported for other proteins [36]. Likewise, a fivefold reduction in *in vitro* potency, with an IC_{50} value of 5.7 nM, was observed for the PEGylated Anticalin in a HUVEC proliferation assay, which otherwise indicated mutually similar IC_{50} values for the unmodified Anticalin and bevacizumab of 1.49 and 1.19 nM, respectively (Fig. 3c).

Inhibition of VEGF-mediated vascular permeability and tumor growth

In addition to its pro-angiogenic effects, VEGF-A increases vascular permeability, and this activity can be assessed by dye extravasation into the skin after intradermal injection [37]. In a first experiment, PRS-050 (not PEGylated) or bevacizumab was each mixed with VEGF-A and injected locally into the skin of guinea pigs, applying different combinations as well as controls on a regular grid (Fig. 4a). As result, both PRS-050 and bevacizumab essentially abolished dye extravasation. Furthermore, when in a different setting PEG40-conjugated PRS-050 was administered intravenously 12 h prior to the intradermal injection of different amounts of VEGF-A, the area of dye extravasation was significantly reduced in the treated animals if compared with a control group (Fig. 4b). These findings clearly indicate that PRS-050 is able to neutralize VEGF-A function *in vivo* after both local and systemic administration.

Next, we investigated the activity of PEG40-conjugated PRS-050 in comparison with bevacizumab in the A673 sarcoma xenograft model [20]. A673 cells were injected *s.c.* into irradiated nude mice, and *i.p.* treatment with VEGF-A antagonists was initiated on the same day. Based on literature data, we chose several bevacizumab doses in order to ascertain that the maximal effect was reached. In line with previous reports, 2–5 mg/kg of the murine predecessor antibody A4.6.1, administered every 3 days, showed optimal tumor suppression in this model [20, 38]. The dosing interval of PRS-050-PEG40, using 7.5 mg/kg, was varied from daily to every 3 days based on the preceding experiment (Fig. 4c).

PEG40-conjugated PRS-050 exhibited a potent antitumor effect at all dosing intervals. Notably, the maximal effect of tumor growth inhibition (TGI = 84 %) that was seen for the Anticalin even seemed to exceed that of bevacizumab in this model. A confirmative investigation with the same mouse model included histopathological assessment of satellite animals ($n = 3$ mice per group). Immunohistochemical (IHC) staining for CD31 served to semiquantitatively determine microvessel density. These satellite mice were killed toward the end of the 3-week treatment period while tumor relapse was followed in the main study groups after cessation of treatment. Tumor growth curves confirmed the activity of PRS-050-PEG40 during the 20-day treatment period, whereas after treatment both the bevacizumab and PRS-050-PEG40 groups showed a comparable relapse of tumor growth (Fig. 4d).

Tumor sections obtained from the satellite animals were subjected to hematoxylin–eosin–safran (HES) staining or IHC analysis for CD31 expression. In the HES-stained sections, the A673 tumors appeared as poorly differentiated

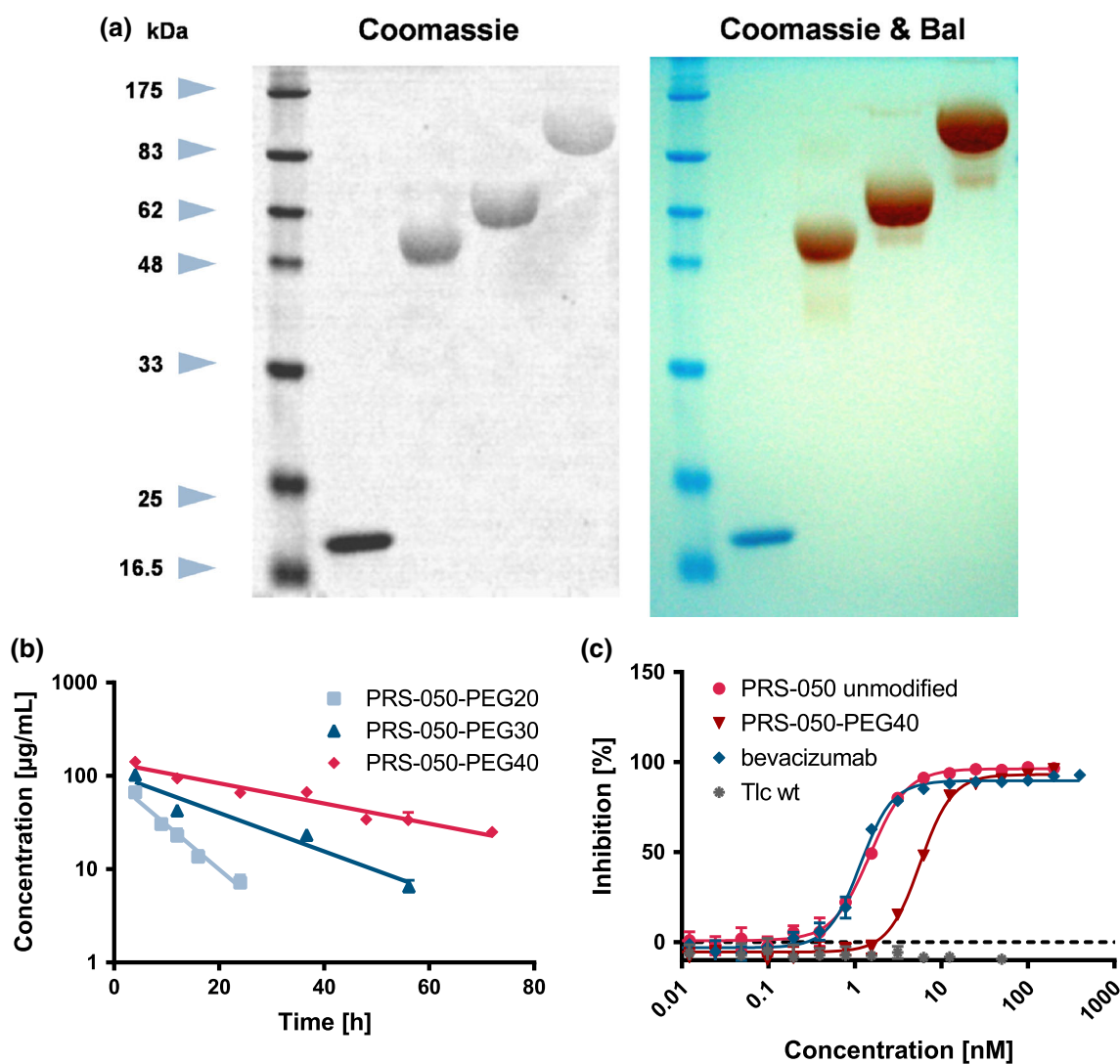


Fig. 3 Purity and pharmacokinetic properties of Anticalin-PEG conjugates. **a** Analysis of the conjugates on SDS-PAGE followed by Coomassie staining for protein as well as combined Coomassie/BaI staining to additionally visualize the PEG component. **b** The PEGylated Anticalins were administered by bolus i.v. injection (10 mg/kg) to female NMRI mice, and the plasma levels were determined by ELISA on VEGF₈₋₁₀₉-coated microtiter plates in blood

samples taken at the indicated time points. Note that concentrations refer to the entire PEG conjugates rather than just the protein component. **c** PEGylated Anticalin was tested side by side with unmodified Anticalin and bevacizumab in a cell viability assay, showing the ability of all three antagonist reagents to inhibit VEGF-A induced stimulation of HUVEC proliferation. Cell viability was quantified using the chemoluminescent CellTiter-Glo assay reagent

Table 1 Key PK parameters of PEGylated PRS-050 determined for mice

Format	i.v. Dose (mg/kg)	AUC _{0-∞} (h $\mu\text{g/mL}$)	V _D (mL/kg)	C _L (mL/h kg)	t _{1/2} (h)
20 kDa PEG	10	1124	130.3	8.90	7.2
30 kDa PEG	10	2230	74.8	4.48	11.8
40 kDa PEG	10	6188	64.8	1.62	28.3

high-grade sarcomas, often with significant areas of necrosis. Comparable histological features and levels of necrosis were observed in all tumors examined, irrespective of the treatment (for a representative image, see Fig. 4e). CD31 staining revealed blood vessels in

continuity with host tissue vessels. In the host tissues around the tumor, blood vessels were numerous, well differentiated and with a well-defined lumen. In contrast, vessels within the tumors appeared less differentiated and with decreased or missing lumen. In the tumor, blood

Table 2 Binding activity of the unmodified Anticalin (PRS-050) and its conjugate with 40 kDa PEG toward human VEGF-A analyzed by surface plasmon resonance (Biacore)

	k_a ($10^4 \text{ M}^{-1} \text{ s}^{-1}$)	k_d (10^{-5} s^{-1})	K_D (pM)
Unmodified Anticalin	15.2 ± 0.0035	2.76 ± 0.017	182 ± 1.1^a
PEGylated Anticalin	2.73 ± 0.0020	2.54 ± 0.053	930 ± 19.4^a

^a Standard error from four measurements

vessel distribution was heterogeneous: Some parts of the tumor were devoid of blood vessels while other parts showed a pronounced density of vessels. These observations were made in all samples, irrespective of the treatment (Fig. 4f). However, tumor blood vessel density was consistently decreased in all treatment groups compared with the vehicle group (Fig. 4g). These results were statistically significant for both PRS-050-PEG40 groups, i.e., irrespective of dosing daily or every second day.

The antitumor activity of PRS-050-PEG40 was further confirmed in U87-MG glioblastoma xenograft mice (TGI = 74 %) and also in established HCT-116 colon carcinoma bearing nude rats in an interventional setting when treatment was initiated at a tumor volume of 400 mm^3 (TGI = 61 %; not shown). Thus, PEG40-conjugated PRS-050 has demonstrated potent antitumor activity across a range of relevant tumor models.

Bevacizumab but not PRS-050 immune complexes induce thrombosis in Fc γ RIIA transgenic mice

Due to their bivalent binding mode, monoclonal antibodies can form stable high molecular weight immune complexes with dimeric target proteins such as VEGF-A. This is especially the case for bevacizumab, whose apical epitope position on VEGF-A prevents bivalent intramolecular binding [39]. Immune complexes formed between bevacizumab and VEGF₁₆₅ were previously shown to activate platelets and to cause platelet granule release and aggregation in vitro and in vivo [27]. This can be mimicked in human Fc γ RIIA transgenic mice, whereas mouse platelets lack the genetic equivalent of the human platelet IgG receptor [40].

The addition of heparin enhances this activity as it binds both VEGF₁₆₅ and the platelets. Nevertheless, the activation of platelets through Fc γ RIIA is strictly dependent on the antibody Fc region. As the monovalent PEG40-conjugated PRS-050 forms well-defined low molecular weight complexes with the homodimeric VEGF₁₆₅ in a 2:2 stoichiometry and does not contain an Fc region, we investigated its side effect profile in comparison with bevacizumab in mice transgenic for human Fc γ RIIA. Indeed, severe thrombocytopenia (Fig. 5a) and pulmonary thrombosis (Fig. 5b) were observed in animals injected

with bevacizumab + VEGF₁₆₅ but not in animals injected with PEG40-conjugated PRS-050 + VEGF₁₆₅, with bevacizumab + VEGF₁₂₁ (which lacks the heparin-binding domain) or with PBS (vehicle control). A significant drop in platelet counts was only observed in the group of animals injected with bevacizumab/VEGF₁₆₅ immune complexes, which indicates severe platelet clearance.

Representative lung sections stained with hematoxylin and eosin (HE) revealed many blood vessels largely occluded by thrombi only occurring in animals injected with bevacizumab + VEGF₁₆₅ (Fig. 5b, lower right, 400 \times magnification). In addition, vast regions of lung tissue exhibited congestion or destruction of the alveolar microvasculature in this group, whereas all other groups showed healthy lung tissue with well-rounded alveoli and normal microvasculature. Furthermore, impaired mobility and apparent neuromuscular spasms were observed in animals injected with bevacizumab + VEGF₁₆₅ but not in any of the other groups, in particular those that had received PRS-050 (not shown). This demonstrates an improved safety profile for the VEGF-A-specific Anticalin in this thrombosis model.

Discussion

We have engineered a VEGF-A-specific Anticalin based on human Tlc as a monomeric small protein that possesses purely antagonistic blocking properties and is devoid of immunological effector functions. In fact, neither the bivalent binding activity of an antibody, such as bevacizumab, nor the immunoglobulin Fc part is required to achieve potent neutralization of this predominantly soluble angiogenic growth factor. From a panel of VEGF-specific mutated lipocalins that were initially selected out of the naive random library via phage display, one candidate was identified that binds all tested splice variants of human VEGF-A with subnanomolar affinity, cross-reacts with rodent VEGF-A and antagonizes binding of VEGF-A to both of its receptors VEGFR-1 and VEGFR-2 on vascular endothelial cells.

Following assessment of the in vitro potency of this Anticalin, we demonstrated its ability to inhibit VEGF-A-induced breakdown of the blood–retinal barrier upon

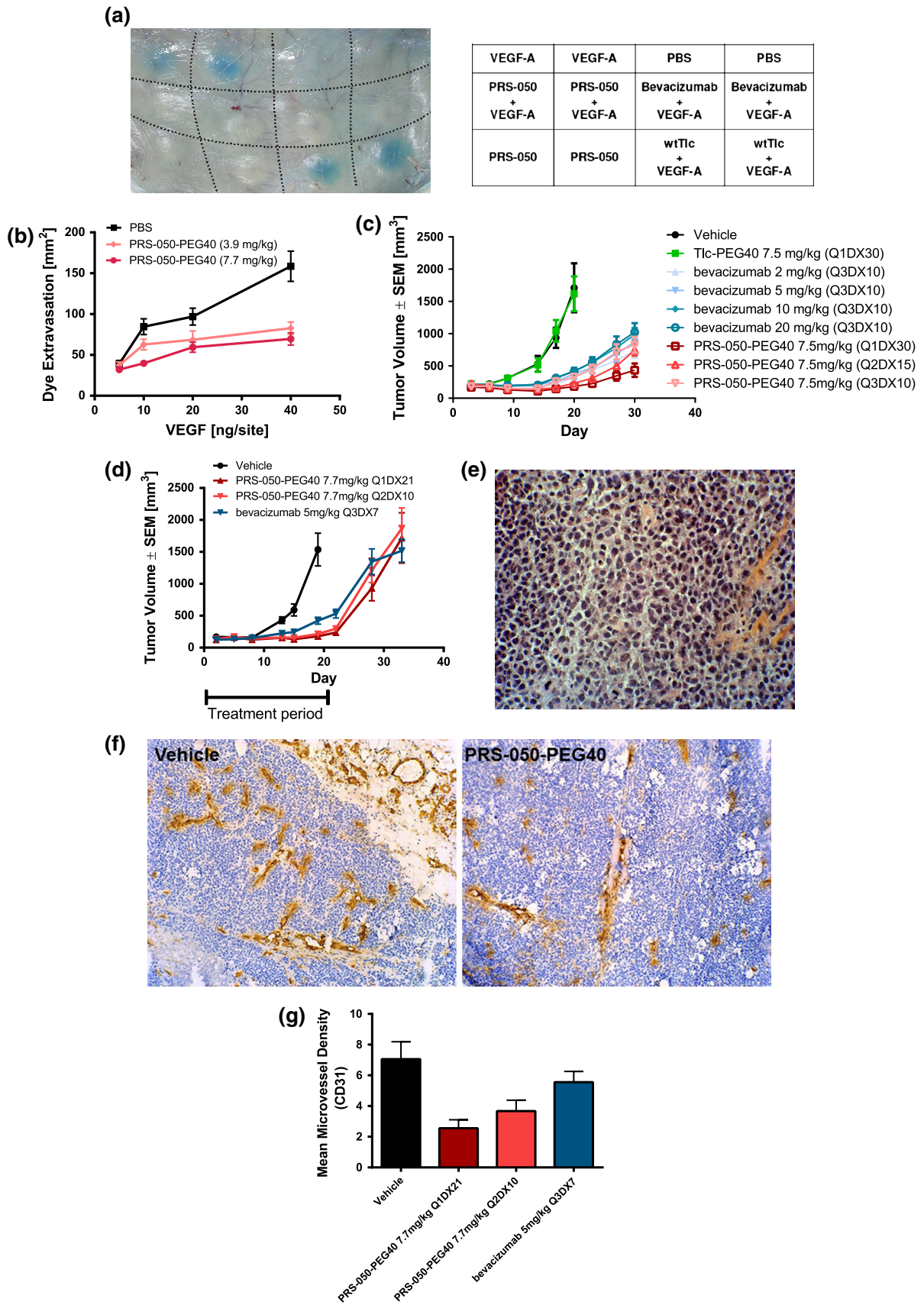


Fig. 4 Inhibition of dye extravasation and tumor growth by PRS-050 in vivo. **a** Unmodified Anticalin (88 ng), wtTlc (88 ng) or bevacizumab (357 ng) was premixed with VEGF-A (20 ng), incubated at room temperature for 30 min, and then injected intradermally (100 μ L/site) on the pre-shaved dorsum of a guinea pig in a 3 \times 4 grid pattern as indicated. **b** Systemic administration of PEG40-conjugated Anticalin at two dose levels 12 h prior to intradermal injection of indicated amounts of VEGF-A. **c** A673 sarcoma xenograft growth curves on nude mice ($n = 10$) treated with PEG40-conjugated PRS-050 or bevacizumab at the indicated dose levels and dosing intervals. **d** A673 sarcoma xenograft growth curves for nude mice treated with PEG40-conjugated PRS-050 or bevacizumab at the indicated dose levels and dosing intervals (each day or every second day). Following cessation of treatment on day 19 (together with removal of the 3 satellite animals), tumor growth was monitored as long as the groups included ≥ 10 animals. **e** A representative hematoxylin–eosin–safran (HES)-stained tumor section from the satellite animals at 400 \times magnification. **f** Anti-CD31-stained sections showing the blood vessel distribution in tumors obtained from the satellite animals treated with vehicle or PRS-50-PEG40 at 100 \times magnification. **g** Enumeration of CD31 stained vessels in the tumor periphery

intravitreal administration to the rabbit eye. The low molecular weight of the Anticalin does not constitute a drawback for ocular applications since the half-life in the vitreous of approximately 3 days is similar to the value published for the significantly larger Fab fragment ranibizumab [34]. On the contrary, the lower molecular weight and, thus, increased specific activity may facilitate the administration of a higher stoichiometric dose of the Anticalin to the vitreous, hence potentially extending the duration of VEGF-A neutralization, e.g., for the treatment of age-related macular degeneration (AMD) or in other ophthalmological indications.

Frequent intravitreal injections not only bear the risk of administration-related ocular complications, including infections, but also cause significant cost and, hence, constitute an important incentive toward developing improved long-lasting antineovascular therapeutics in ophthalmology [41]. Better tissue penetration of small proteins has been reported for the back of the eye in rhesus monkeys [42], and this may also translate into an advantage of our Anticalin. On the other hand, systemic exposure to the Anticalin after its diffusion into circulation is expected to be low due to the rapid renal filtration of the 20 kDa protein.

Conversely, to allow persistent systemic inhibition of VEGF-A, e.g., for applications in oncology, the plasma half-life of the Anticalin was extended by site-directed PEGylation. To this end, a free exposed cysteine residue was introduced at the protein surface of the Anticalin, facing away from the presumed VEGF-A-binding site, for site-directed conjugation with polyethylene glycol (PEG) of different chain lengths and complexity. A branched 40 kDa PEG moiety conferred a plasma half-life of more than one day in mice while a half-life of even 5.5–7 days

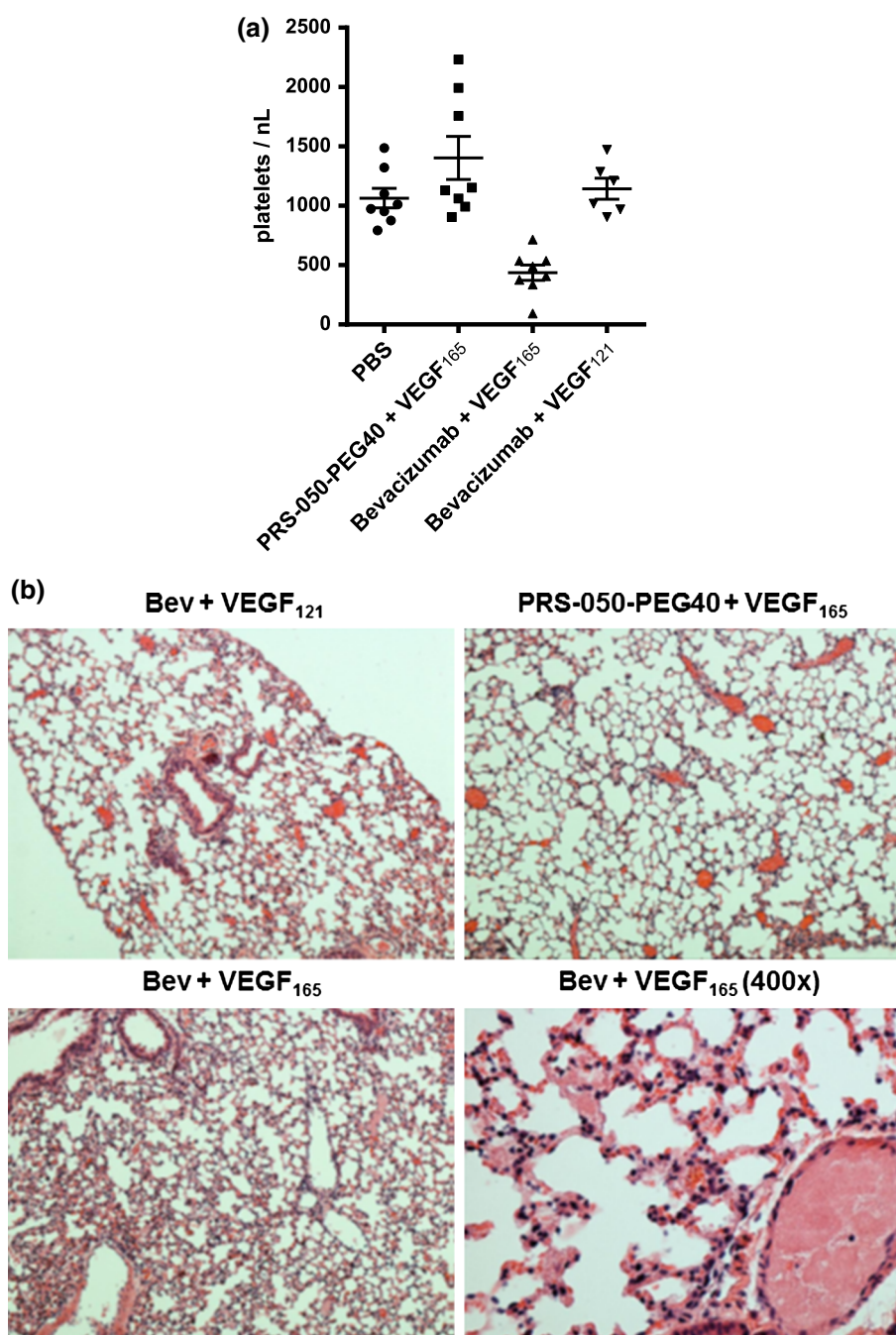
has been observed for this conjugate in humans [43]. The PEGylated Anticalin demonstrated excellent in vivo antagonistic activity, both blocking the effect of VEGF-A on dye extravasation in the Miles guinea pig model and strongly inhibiting tumor xenograft growth in several mouse and rat models.

In fact, in an A673 xenograft experiment the PEG40-conjugated PRS-050 appeared more efficacious than the established biopharmaceutical bevacizumab even though the Anticalin has a shorter plasma half-life in mice compared with the antibody (6.8 days [44]). However, the better suppression of tumor growth in this animal model may be due to the fact that both the tumor-derived (i.e., human) VEGF-A and the murine stromal VEGF promote tumor growth [45, 46]. In contrast to PRS-050, bevacizumab is unable to neutralize murine VEGF [47]. Nevertheless, in the human pathological situation other factors also may come into play, which should lead to pharmacodynamic properties of the Anticalin different from antibodies: for example, better tissue penetration, the absence of multimeric immune complexes (see below), the lack of binding to Fc receptors, and the overall faster elimination of the 2:2 drug:target complex via the kidney.

In this regard, it should be kept in mind that the physiological set of VEGF-A proteins comprises multiple splice forms and proteolytically processed isoforms. The complexity of this system is further enhanced by the presence of multiple VEGF-A receptors in addition to VEGFR-2, such as VEGFR-1 and the neuropilins, as well as low affinity interactions of the heparin-binding domain in a subset of VEGF-A isoforms with the extracellular matrix [48]. While all cell-based experiments reported here were conducted with a constant concentration of human VEGF₁₆₅, it has to be considered that differences in the endothelial responses may occur depending not only on VEGF-A concentration and/or duration of exposure but also on the temporal gradient of exposure [49]. Ultimately, in accordance with simulations of the effects of VEGF-neutralizing agents in the context of multiple ligand–receptor interactions [50], the response to any neutralizing VEGF-A reagent will be determined by the local free ligand concentration in the tumor microenvironment over time.

Generally, Anticalins offer advantages over antibodies in instances where Fc-mediated functions are neither required nor desired, and the sole purpose of the therapeutic intervention consists in blocking of a pathological receptor–ligand interaction [4]. Due to their truly monovalent nature, Anticalins are not expected to form multimeric complexes as they often result from the interaction between antibodies and oligomeric antigens, such as described for bevacizumab and adalimumab [51]. Notably, a causal role of such immune complexes in thrombocytopenia and adverse thromboembolic events has been observed occasionally with

Fig. 5 Immune complexes formed by bevacizumab but not by PEG40-conjugated PRS-050 induce thrombosis in Fc γ RIIa transgenic mice. **a** Platelet counts from individual mice 10 min after injection with PBS ($n = 8$) or with one of the following immune complexes: PEG40-conjugated PRS-050 + VEGF₁₆₅ ($n = 8$), bevacizumab + VEGF₁₆₅ ($n = 8$), bevacizumab + VEGF₁₂₁ ($n = 6$). **b** Representative lung sections from corresponding animals stained with hematoxylin and eosin (HE) at 100 \times magnification (or 400 \times for close-up view)



bevacizumab [25, 52, 53]. Furthermore, antibody immune complexes with VEGF-A can deposit in the kidney glomeruli where they may lead to complement C3 accumulation and glomerulosclerosis, in particular with antibody versions having enhanced affinity [26]. As demonstrated here in mice transgenic for the human platelet IgG receptor, Fc γ RIIa, PRS-050 administered together with VEGF₁₆₅ did neither trigger platelet aggregation nor thrombosis, which suggests an improved safety profile.

Anticalins can be derived from human lipocalin family members such as Tlc (Lcn1) or NGAL (Lcn2), among others [4], and they share approximately 90 % amino acid sequence identity with their abundant endogenous counterparts. Thus, the risk of eliciting immunogenic effects upon administration to human patients should be low. Only the mutagenized loop regions may represent new epitopes, which can, however, be assessed *in silico* using current bioinformatic tools [54]. In fact, no antidrug antibody (ADA) responses were

detected in a recent phase I clinical trial of PRS-050 even in patients that had received multiple doses [43].

Our work highlights that functional engineering of human lipocalins can be readily achieved, yielding Anticalins with the potential to be developed as therapeutic proteins for medical therapy and, thus, establishing a new drug platform. Due to the small molecular size, compact structure and intrinsic stability, PRS-050 and its derivatives should offer protein drugs with enhanced penetration into neovascularized tissues. Along this line, the PEGylated PRS-050 Anticalin has demonstrated dose-proportional pharmacokinetics and expected pharmacodynamic effects in patients with solid tumors while it was generally well tolerated [43].

Methods

VEGF_{8–109} production

A synthetic gene encoding amino acid residues 8–109 of human VEGF-A was subcloned on the T7 promoter vector pET11c and expressed in *E. coli* BL21(DE3) in shake flasks according to a published procedure [28]. Inclusion bodies were collected after sonication, washed and solubilized in 20 mM Tris–HCl pH 7.5, 4 mM DTT, 7.5 M urea. Following centrifugation, the supernatant was sterile-filtered, and refolding was initiated by dialysis against 20 mM Tris–HCl pH 8.4, 400 mM NaCl, 1 mM cysteine, followed by 20 mM Tris–HCl pH 8.4, 1 mM cysteine and, finally, 20 mM Tris–HCl pH 8.4. The recombinant protein was further purified by anion-exchange chromatography on Q-Sepharose as well as Superdex 75 size-exclusion chromatography. Its correct folding was confirmed in an ELISA by measuring VEGF-R2 binding activity.

Generation of phagemid library

A random library of Tlc was prepared by concerted mutagenesis of 18 selected amino acid positions located in the 4 loops of the mature human lipocalin 1. To this end, a gene cassette wherein the corresponding codons were randomized in a targeted fashion was assembled via polymerase chain reaction (PCR) with degenerate primer oligodeoxynucleotides in two steps according to a strategy described before [29]. In this library design, the four N-terminal amino acid residues (HHLA) as well as the two C-terminal residues (SD) of the Tlc wild-type sequence were deleted [55]. Also, the natural disulfide bridge of Tlc was eliminated by exchange of the two corresponding cysteine residues at positions 61 and 153 by serine. In order to implement a pair of unique *Bst*XI restriction sites at both sides of the central coding region

for the purpose of efficient cloning, two further mutations were introduced: Arg111 → Pro and Lys114 → Trp.

To generate the random library, first a PCR fragment with randomized codons for the first and second exposed loops of Tlc was prepared, while another PCR fragment with randomized codons for the third and fourth exposed loops was prepared in parallel. In the second step, these two PCR fragments were combined with a connecting oligodeoxynucleotide and used as templates in a PCR to yield the assembled randomized gene cassette in a similar way as described before [12].

For subsequent cloning, the fragment representing the randomized central part of the Tlc coding region was cut with *Bst*XI, and incompletely digested DNA fragments were removed via 5'-biotin tags using streptavidin-coated paramagnetic beads (Merck). In the following ligation reaction, the mutagenized library cassette was inserted into an appropriate *E. coli* phasmid vector, and a phagemid display library comprising 2.0×10^9 variants was prepared according to a published procedure [29].

Anticalin selection and screening ELISA

The Tlc-based random library was subjected to four cycles of filamentous phage display selection against the biotinylated recombinant VEGF_{8–109} from above. The target protein was incubated in solution at a concentration of 200 nM with 2×10^{12} phagemids previously blocked with bovine serum albumin (BSA). Target-bound phagemids were then captured via streptavidin-coated paramagnetic beads, followed by 8 washing steps and competitive elution in the presence of 42 μM unbiotinylated target for 2 h. Phagemid amplification between panning cycles was performed as described before [56]. Enriched clones were individually expressed at small scale in the periplasm of *E. coli* followed by high-throughput (HT) ELISA screening of the soluble proteins, which led to the identification of a candidate Anticalin that competitively inhibited the interaction between VEGF-A and VEGFR-2.

The affinity of this initial Tlc variant was further improved in two cycles of in vitro evolution, by amplifying the central part of its coding region via error-prone polymerase chain reaction (PCR), followed by phage display selection and HT-ELISA screening with the same target as before. During these experiments, a lower target protein concentration and also a shorter incubation time for the interaction with phagemids were used to increase the stringency of selection. For HT-screening ELISA, Tlc variants equipped with a T7 tag (Novagen) as well as the *Strep*-tag II (IBA) were expressed as soluble proteins in a 96-well microtiter plate using the *E. coli* strain TG1/F[–] [57]. Anticalin expression was induced at OD₅₅₀ = 0.6

with 1.2 µg/ml anhydrotetracycline overnight at 22 °C and 700 rpm. Afterward, cells were lysed by addition of one volume 400 mM Na-borate, pH 8.0, 320 mM NaCl, 4 mM EDTA, 0.3 % lysozyme for 1 h under agitation. The crude extract was blocked by addition of 2 % BSA and 0.05 % Tween 20 and tested in an ELISA for binding to VEGF-A as well as suitable control proteins.

Anticalin production and PEGylation

The Anticalin PRS-050 was expressed in *E. coli* W3110 from a pASK75 [58] derivative using the OmpA signal peptide. After preparation of the periplasmic cell extract, the protein was purified to homogeneity via chromatography on *Strep-Tactin* affinity resin (IBA) as well as anion-exchange and size-exclusion chromatography. Purity was assessed by SDS-PAGE on 14 % precast gels (Novex) after Coomassie staining. Whenever the protein was designated for prospective intravitreal use, filtration through a Mustang E cartridge (PALL) in PBS was performed to deplete endotoxin according to the manufacturer's recommendations.

A version of the Anticalin carrying a free cysteine residue was prepared in the same manner. In this case, the thiol side chain was activated by addition of tris(2-carboxyethyl) phosphine (TCEP) at twofold molar amount. The mixture was allowed to react under moderate agitation for 2–4 h at room temperature. Subsequently, maleimide-activated PEG (NOF) was added at 1:1 stoichiometric ratio directly to the reaction mixture. Conjugation was performed for 2–3 h at room temperature. Unreacted PEG and unconjugated protein were removed by cation-exchange chromatography on Macro Cap SP resin at pH 5 using a NaCl gradient for elution. The protein concentration was adjusted to 3.0 mg/mL by diafiltration against PBS, and purity was assessed by SDS-PAGE and RP-HPLC on a C18 column (Phenomenex).

Real-time analysis of ligand binding (Biacore)

SPR spectroscopy was performed on a Biacore T100 instrument (GE Healthcare) at 25 °C to characterize binding activity and specificity of the Anticalins. VEGF_{8–109} was immobilized on a CM5 sensorchip surface using amine coupling chemistry, yielding approximately $\Delta\text{RU} = 600$. Anticalin analyte solutions, either for the unmodified protein or for the PEGylated version, were then applied in dilution series at concentrations of 5, 15, 45, 135 nM and 25, 75, 225, 675 nM, respectively, with HBS-EP (GE Healthcare) as running buffer. The following instrument parameters were used: contact time 120 s, dissociation time 1000 s, flow rate 30 mL/min. Regeneration of the chip surface between measurements was accomplished with 10 mM glycine/HCl pH 1.5. Data evaluation was carried out with the

Biaevaluation software using double referencing. The equilibrium dissociation constant K_D and its standard error were derived as previously described [13]. For practical reasons, the assay was inverted for assessment of interactions with VEGF orthologs and isoforms with the unmodified Anticalin; thus, with the Anticalin protein immobilized to the sensorchip, each of the VEGF molecules could be tested on the same binding surface.

Cell-based characterization using primary endothelial cells

Pooled HUVECs (Promocell) were grown in the supplier's ECB medium with growth factors and supplements according to the supplier's instructions, and used between passage 2 and 6. For the phospho-ERK1/2 quantification, 4000 cells were seeded per well in a 96-well microtiter plate, each with 100 µL full medium (Promocell), on day one. On the following day, the medium was removed and replaced with ECB, 0.5 % FCS without growth factors or other medium supplements and cells were starved for 16 h. On day 3, the medium was replaced with ECB, 0.5 % BSA and starvation was continued under these more stringent conditions for 3 h. Cells were stimulated in ECB containing 0.5 % BSA with 20 ng/mL VEGF₁₆₅ (R&D Systems), which had been pre-incubated at 37 °C for 30 min with Anticalin or bevacizumab (Avastin, Genentech/Roche) in appropriate amounts to yield the indicated final antagonist concentrations. Stimulation was terminated after 10 min, and, after fixation and permeabilization, cells were analyzed for ERK1/2 phosphorylation using a FACE ERK1/2 cell-based ELISA (Active Motif).

For the viability assays, 850 cells were seeded per well in white, optical bottom 96-well plates in 80 µL ECB, 0.5 % FCS lacking growth factors and supplements. Plates were incubated at 37 °C for 1 h until cells had attached. Anticalin and antibody dilutions were prepared in 20 µL of the same starvation medium with VEGF₁₆₅ (R&D systems) or FGF-2 (ReliaTech). After 30-min pre-incubation at room temperature, the mixtures were added to the cells to yield final concentrations of 20 ng/mL VEGF or 100 ng/mL FGF-2. On day 6, viability was measured using the chemoluminescent CellTiter-Glo assay (Promega).

Mouse pharmacokinetic studies

Female NMRI mice were dosed intravenously with PRS-050 conjugated to 20, 30 or 40 kDa PEG. 0.5 mL of blood samples was taken from the retro-orbital plexus of three mice per compound and time point under slight anesthesia and transferred immediately into lithium–heparin-containing vials, followed by manual mixing. Samples were stored on ice until centrifugation. PRS-050 levels were

determined from the resulting plasma preparations using the sandwich ELISA described below except that the assay was performed in 20 % mouse plasma.

Ocular pharmacokinetics

100 μ L of 1 mg/mL PRS-050 in PBS was injected into the mid-vitreous of both eyes of 16 anesthetized pigmented rabbits. After 0.25, 1, 2, 4, 8, 11, 14, 16 days, each 2 animals were euthanized and the vitreous was prepared from both eyes. Vitreal concentrations of functionally active PRS-050 were determined using a sandwich ELISA. Briefly, ELISA plates were coated with the recombinant VEGF₈₋₁₀₉ at 5 μ g/mL in PBS for 1 h at room temperature. Plates were washed 6 times with PBS, 0.05 % Tween 20 and blocked in PBS, 0.1 % Tween 20, 3 % skim milk powder for 2 h at room temperature. Plates were again washed 6 times in PBS, 0.05 % Tween 20. Samples were assayed in three dilutions in duplicate. Unknowns, standards and quality controls were captured for 1 h at room temperature on the plates at a vitreous matrix concentration of 20 % in PBS, 0.05 % Tween 20, 0.5 % BSA. Blank matrix was harvested in-house from locally procured rabbit eyes. Following 6 washes in PBS, 0.05 % Tween 20, biotinylated goat anti-lipocalin 1 antiserum (R&D Systems) was added at 0.31 μ g/mL in PBS, 0.1 % Tween 20 for 1 h. Plates were washed as before, and Extravidin-HRP (Sigma) was added at a 1:10,000 dilution in PBS, 0.1 % Tween 20 for 1 h. After 6 washes, detection was achieved using QuantaBlu (Pierce) according to the manufacturer's instructions. Microwin software was used for data analysis.

Inhibition of blood–retinal barrier breakdown

Twenty pigmented rabbits were randomly divided into 4 groups. On day 1, 100 μ g PRS-050, 100 μ g bacterially produced wtTlc, 300 μ g ranibizumab (Lucentis, Novartis) or PBS were injected into the mid-vitreous of the right eye of each anesthetized animal using a 30G needle. On day 6, right eyes were injected intravitreally with 500 ng rhVEGF₁₆₅ (R&D Systems) to induce increased retinal vascular permeability. 47 h after VEGF challenge (on day 8), sodium fluorescein (0.9 %, 50 mg/kg) was injected via the marginal ear vein into all animals. 1 h thereafter, ocular fluorescein levels in both eyes were determined using a Fluorotron Master ocular photometer (OcuMetrics). A series of scans consisting of 148 steps were performed from the cornea to the retina along the optical axis. The area under the curve (AUC) was calculated from the fluorescence intensities using the trapezoidal rule for each eye for the vitreoretinal and anterior (aqueous humor and cornea) segments. Results were expressed as the ratio of the AUC between the right (treated) eye and the left (untreated) eye.

Miles assay

Vascular permeability was assessed using a modified Miles dye extravasation assay [59]. Male Duncan-Hartley guinea pigs of 320 ± 20 g weight were shaved on the shoulder and back region prior to the experiment and received an intravenous injection of 1 mL 1 % Evans Blue. 30 min later, rhVEGF₁₆₅ which had been premixed with antagonists or controls was injected intradermally. For systemic antagonist administration, Anticalin or control was injected into the ear vein 12 h prior to the experiment ($n = 3$ per group). Injections of 5, 10, 20 and 40 ng rhVEGF₁₆₅ were permuted, using a 3×4 grid pattern, with respect to head/tail and spine on each guinea pig. 60 min after VEGF injection, the animals were euthanized by CO₂ asphyxiation and the skin containing the grid pattern was prepared, cleaned of connective tissue and photographed. The areas of Evans Blue extravasation around the injection sites were traced onto clear plastic sheets and quantified with Image Pro Plus 1.3 software (Media Cybernetics).

A673 xenograft model

The human A673 sarcoma cell line (ATCC) was grown in DMEM, 10 % FCS. On the day before inoculation, 90 SWISS nude mice were whole body irradiated with a Co⁶⁰ γ -source (2.5 Gy). Tumors were induced subcutaneously by injection of 1×10^7 cells in 200 μ L of a 1:1 mix of DMEM and matrigel (BD Bioscience). On the same day, mice were randomized into groups of 10 based on body weight, and treatment was initiated (day 0). Mice were treated with intraperitoneal injections of PEG40-conjugated PRS-050 or bevacizumab at various dose levels, between 2 and 20 mg/kg, using 10 mL/kg dose volume. Control groups were dosed with PBS vehicle or PEG40-conjugated wtTlc. Tumor size was measured twice weekly with a caliper, and the tumor volume was approximated by the formula $(\text{length} \times \text{width}^2)/2$ [60]. Mice were killed once the tumor volume reached 2000 mm³ or on day 30 at the latest. A necropsy involving macroscopic examination of heart, lungs, liver, spleen, kidneys and gastrointestinal tract was performed for all killed mice and did not reveal any pathological findings. For the confirmatory experiment, 15 mice were included per group, 3 of which served as satellite animals in each treatment arm. These were killed on day 19 of the study, and tumors were collected. The tumor tissue was cryoprotected in O.C.T. compound (Tissue-Tek) and sectioned. One tumor section (6–8 μ m thickness) per block was mounted on glass slides and stained with hematoxylin–eosin–safran (HES).

For CD31 immunostaining, three sections taken at different levels were investigated for each block. After mounting on glass slides, dried tissue sections were treated

with methanol containing 3 % hydrogen peroxide. The primary rat anti-mouse CD31 antibody (BD Biosciences) was applied at 1/50 dilution for 60 min at 25 °C. All slides were counterstained with hematoxylin. For each tumor, CD31-stained blood vessel density was counted in six areas located in the tumor periphery and examined at 400× magnification under an Olympus BH2 microscope. The U Mann–Whitney nonparametric test was used for statistical analysis.

Immune complex-induced thrombosis in human FcγRIIa transgenic mice

Six eight-week-old human FcγRIIa transgenic mice [B6;SJL-Tg(FCGR2A)11MKZ/J], bred and genotyped at the Florida Hospital Center for Thrombosis Research, were used in an acute immune complex-induced thrombosis model essentially as described [27]. Briefly, transgenic mice were injected into the lateral vein ($n = 6–8$ /group) with immune complexes or, as control vehicle, PBS (0.2 mL). Immune complexes were preformed *in vitro* by mixing equimolar amounts of either PEG40-conjugated PRS-050 or bevacizumab with 42 μg rhVEGF₁₆₅ in PBS with addition of 0.6 IU unfractionated heparin for 30 min at room temperature. Another group was injected with immune complexes prepared from bevacizumab and 28 μg rhVEGF₁₂₁ (R&D Systems). The animals were monitored with video recording for visible signs of thrombotic phenotype and killed after 10 min. Blood was drawn by cardiac puncture from anesthetized mice into 0.1 mL of 3.2 % trisodium citrate, and platelets were quantified using a Coulter AcT-diff cell counter. In addition, lungs from 3 animals per group were dissected, rinsed in PBS and fixed with formalin (24 h). Tissue sections were processed by the Florida Hospital Main Laboratory, Pathology Division, in an automated HE staining process, and HE sections were photographed on a microscope and analyzed for evidence of thrombosis.

Acknowledgments We are indebted to all current and previous members of the Pieris team, in particular Steffen Schlehuber and Antje Walz, for their contributions and support. We are also grateful to Shane Olwill and Ulrich Moebius for critical reading of the manuscript.

Author contributions H. G., A. M. H., G. M., M. H., L. P. A. and A. S. designed experiments. H. G., M. H., S. T., G. M., H. J. C. and S. T. performed experiments and analyzed the data. T. M. and A. A. designed, performed and analyzed the experiments in FcγIIa transgenic mice. H. G., A. M. H., L. P. A. and A. S. wrote the manuscript.

Compliance with ethical standards

Conflict of interest G. M. is a full-time employee at Pieris Pharmaceuticals GmbH. H. G., M. H., S. T., H.-J. C., A. M. H. and L. P. A. were full-time employees of Pieris AG. A. S. is founder of Pieris AG and shareholder of Pieris Pharmaceuticals, Inc.

Ethical standards All experiments described in this manuscript comply with the laws of the USA and the European Union. All animal experiments were reviewed and approved by the responsible animal ethics committees.

References

- Nelson AL, Dhimolea E, Reichert JM (2010) Development trends for human monoclonal antibody therapeutics. *Nat Rev Drug Discov* 9:767–774
- Reichert JM (2014) Antibodies to watch in 2014. *mAbs* 6:5–14
- Skerra A (2007) Alternative non-antibody scaffolds for molecular recognition. *Curr Opin Biotechnol* 18:295–304
- Richter A, Eggenstein E, Skerra A (2014) Anticalins: exploiting a non-Ig scaffold with hypervariable loops for the engineering of binding proteins. *FEBS Lett* 588:213–218
- Åkerström B, Borregaard N, Flower DR, Salier J-S (2006) Lipocalins. *Landes Bioscience, Georgetown*
- Skerra A (2000) Lipocalins as a scaffold. *Biochim Biophys Acta* 1482:337–350
- Schiefner A, Skerra A (2015) The menagerie of human lipocalins: a natural protein scaffold for molecular recognition of physiological compounds. *Acc Chem Res* 48:976–985
- Newcomer ME, Jones TA, Aqvist J, Sundelin J, Eriksson U, Rask L, Peterson PA (1984) The three-dimensional structure of retinol-binding protein. *EMBO J* 3:1451–1454
- Goetz DH, Holmes MA, Borregaard N, Bluhm ME, Raymond KN, Strong RK (2002) The neutrophil lipocalin NGAL is a bacteriostatic agent that interferes with siderophore-mediated iron acquisition. *Mol Cell* 10:1033–1043
- Fluckinger M, Haas H, Merschak P, Glasgow BJ, Redl B (2004) Human tear lipocalin exhibits antimicrobial activity by scavenging microbial siderophores. *Antimicrob Agents Chemother* 48:3367–3372
- Flo TH, Smith KD, Sato S, Rodriguez DJ, Holmes MA, Strong RK, Akira S, Aderem A (2004) Lipocalin 2 mediates an innate immune response to bacterial infection by sequestering iron. *Nature* 432:917–921
- Beste G, Schmidt FS, Stibora T, Skerra A (1999) Small antibody-like proteins with prescribed ligand specificities derived from the lipocalin fold. *Proc Natl Acad Sci USA* 96:1898–1903
- Schönfeld D, Matschiner G, Chatwell L, Trentmann S, Gille H, Hülsmeier M, Brown N, Kaye PM, Schlehuber S, Hohlbaum AM, Skerra A (2009) An engineered lipocalin specific for CTLA-4 reveals a combining site with structural and conformational features similar to antibodies. *Proc Natl Acad Sci USA* 106:8198–8203
- Gebauer M, Schiefner A, Matschiner G, Skerra A (2013) Combinatorial design of an Anticalin directed against the extra-domain B for the specific targeting of oncofetal fibronectin. *J Mol Biol* 425:780–802
- Redl B (2000) Human tear lipocalin. *Biochim Biophys Acta* 1482:241–248
- Breustedt DA, Korndörfer IP, Redl B, Skerra A (2005) The 1.8-Å crystal structure of human tear lipocalin reveals an extended branched cavity with capacity for multiple ligands. *J Biol Chem* 280:484–493
- Breustedt DA, Chatwell L, Skerra A (2009) A new crystal form of human tear lipocalin reveals high flexibility in the loop region and induced fit in the ligand cavity. *Acta Crystallogr D Biol Crystallogr* 65:1118–1125
- Olwill SA, Joffroy C, Gille H, Vigna E, Matschiner G, Allersdorfer A, Lunde BM, Jaworski J, Burrows JF, Chiriaco C, Christian HJ, Hülsmeier M, Trentmann S, Jensen K, Hohlbaum

- AM, Audoly L (2013) A highly potent and specific MET therapeutic protein antagonist with both ligand-dependent and ligand-independent activity. *Mol Cancer Ther* 12:2459–2471
19. Ferrara N, Gerber HP, LeCouter J (2003) The biology of VEGF and its receptors. *Nat Med* 9:669–676
 20. Kim KJ, Li B, Winer J, Armanini M, Gillett N, Phillips HS, Ferrara N (1993) Inhibition of vascular endothelial growth factor-induced angiogenesis suppresses tumour growth in vivo. *Nature* 362:841–844
 21. Shojaei F, Ferrara N (2007) Antiangiogenesis to treat cancer and intraocular neovascular disorders. *Lab Invest* 87:227–230
 22. Ferrara N, Hillan KJ, Gerber HP, Novotny W (2004) Discovery and development of bevacizumab, an anti-VEGF antibody for treating cancer. *Nat Rev Drug Discov* 3:391–400
 23. Nalluri SR, Chu D, Keresztes R, Zhu X, Wu S (2008) Risk of venous thromboembolism with the angiogenesis inhibitor bevacizumab in cancer patients: a meta-analysis. *JAMA* 300:2277–2285
 24. Scappaticci FA, Skillings JR, Holden SN, Gerber HP, Miller K, Kabbinavar F, Bergsland E, Ngai J, Holmgren E, Wang J, Hurwitz H (2007) Arterial thromboembolic events in patients with metastatic carcinoma treated with chemotherapy and bevacizumab. *J Natl Cancer Inst* 99:1232–1239
 25. Rudge JS, Holash J, Hylton D, Russell M, Jiang S, Leidich R, Papadopoulos N, Pyles EA, Torri A, Wiegand SJ, Thurston G, Stahl N, Yancopoulos GD (2007) VEGF Trap complex formation measures production rates of VEGF, providing a biomarker for predicting efficacious angiogenic blockade. *Proc Natl Acad Sci USA* 104:18363–18370
 26. Gerber HP, Wu X, Yu L, Wiesmann C, Liang XH, Lee CV, Fuh G, Olsson C, Damico L, Xie D, Meng YG, Gutierrez J, Corpuz R, Li B, Hall L, Rangell L, Ferrando R, Lowman H, Peale F, Ferrara N (2007) Mice expressing a humanized form of VEGF-A may provide insights into the safety and efficacy of anti-VEGF antibodies. *Proc Natl Acad Sci USA* 104:3478–3483
 27. Meyer T, Robles-Carrillo L, Robson T, Langer F, Desai H, Davila M, Amaya M, Francis JL, Amirkhosravi A (2009) Bevacizumab immune complexes activate platelets and induce thrombosis in FCGR2A transgenic mice. *J Thromb Haemost* 7:171–181
 28. Christinger HW, Muller YA, Berleau LT, Keyt BA, Cunningham BC, Ferrara N, de Vos AM (1996) Crystallization of the receptor binding domain of vascular endothelial growth factor. *Proteins* 26:353–357
 29. Skerra A (2001) ‘Anticalins’: a new class of engineered ligand-binding proteins with antibody-like properties. *J Biotechnol* 74:257–275
 30. Gille H, Kowalski J, Li B, LeCouter J, Moffat B, Zioncheck TF, Pelletier N, Ferrara N (2001) Analysis of biological effects and signaling properties of Flt-1 (VEGFR-1) and KDR (VEGFR-2). A reassessment using novel receptor-specific vascular endothelial growth factor mutants. *J Biol Chem* 276:3222–3230
 31. Miyamoto K, Khosrof S, Bursell SE, Moromizato Y, Aiello LP, Ogura Y, Adamis AP (2000) Vascular endothelial growth factor (VEGF)-induced retinal vascular permeability is mediated by intercellular adhesion molecule-1 (ICAM-1). *Am J Pathol* 156:1733–1739
 32. Tolentino MJ, Miller JW, Gragoudas ES, Jakobiec FA, Flynn E, Chatzistefanou K, Ferrara N, Adamis AP (1996) Intravitreal injections of vascular endothelial growth factor produce retinal ischemia and microangiopathy in an adult primate. *Ophthalmology* 103:1820–1828
 33. Narayanan R, Kuppermann BD, Jones C, Kirkpatrick P (2006) Ranibizumab. *Nat Rev Drug Discov* 5:815–816
 34. Bakri SJ, Snyder MR, Reid JM, Pulido JS, Ezzat MK, Singh RJ (2007) Pharmacokinetics of intravitreal ranibizumab (Lucentis). *Ophthalmology* 114:2179–2182
 35. Roberts MJ, Bentley MD, Harris JM (2002) Chemistry for peptide and protein PEGylation. *Adv Drug Deliv Rev* 54:459–476
 36. Kubetzko S, Sarkar CA, Plückthun A (2005) Protein PEGylation decreases observed target association rates via a dual blocking mechanism. *Mol Pharmacol* 68:1439–1454
 37. Dvorak HF, Brown LF, Detmar M, Dvorak AM (1995) Vascular permeability factor/vascular endothelial growth factor, microvascular hyperpermeability, and angiogenesis. *Am J Pathol* 146:1029–1039
 38. Mordenti J, Thomsen K, Licko V, Chen H, Meng YG, Ferrara N (1999) Efficacy and concentration-response of murine anti-VEGF monoclonal antibody in tumor-bearing mice and extrapolation to humans. *Toxicol Pathol* 27:14–21
 39. Muller YA, Chen Y, Christinger HW, Li B, Cunningham BC, Lowman HB, de Vos AM (1998) VEGF and the Fab fragment of a humanized neutralizing antibody: crystal structure of the complex at 2.4 Å resolution and mutational analysis of the interface. *Structure* 6:1153–1167
 40. McKenzie SE, Taylor SM, Malladi P, Yuhan H, Cassel DL, Chien P, Schwartz E, Schreiber AD, Surrey S, Reilly MP (1999) The role of the human Fc receptor FcγRIIA in the immune clearance of platelets: a transgenic mouse model. *J Immunol* 162:4311–4318
 41. Stahl A, Stumpp MT, Schlegel A, Ekawardhani S, Lehrling C, Martin G, Gulotti-Georgieva M, Villemagne D, Forrer P, Agostini HT, Binz HK (2013) Highly potent VEGF-A-antagonistic DARPin as anti-angiogenic agents for topical and intravitreal applications. *Angiogenesis* 16:101–111
 42. Mordenti J, Cuthbertson RA, Ferrara N, Thomsen K, Berleau L, Licko V, Allen PC, Valverde CR, Meng YG, Fei DT, Fourre KM, Ryan AM (1999) Comparisons of the intraocular tissue distribution, pharmacokinetics, and safety of ¹²⁵I-labeled full-length and Fab antibodies in rhesus monkeys following intravitreal administration. *Toxicol Pathol* 27:536–544
 43. Mross K, Richly H, Fischer R, Scharf D, Buchert M, Stern A, Gille H, Audoly LP, Scheulen ME (2013) First-in-human phase I study of PRS-050 (Angiocel), an Anticalin targeting and antagonizing VEGF-A, in patients with advanced solid tumors. *PLoS One* 8:e83232
 44. EPAR (2006) Avastin: EPAR—Scientific Discussion. European Medicines Agency; http://www.ema.europa.eu/docs/en_GB/document_library/EPAR_-_Scientific_Discussion/human/000582/WC500029262.pdf
 45. Gerber HP, Kowalski J, Sherman D, Eberhard DA, Ferrara N (2000) Complete inhibition of rhabdomyosarcoma xenograft growth and neovascularization requires blockade of both tumor and host vascular endothelial growth factor. *Cancer Res* 60:6253–6258
 46. Liang WC, Wu X, Peale FV, Lee CV, Meng YG, Gutierrez J, Fu L, Malik AK, Gerber HP, Ferrara N, Fuh G (2006) Cross-species vascular endothelial growth factor (VEGF)-blocking antibodies completely inhibit the growth of human tumor xenografts and measure the contribution of stromal VEGF. *J Biol Chem* 281:951–961
 47. Yu L, Wu X, Cheng Z, Lee CV, LeCouter J, Campa C, Fuh G, Lowman H, Ferrara N (2008) Interaction between bevacizumab and murine VEGF-A: a reassessment. *Invest Ophthalmol Vis Sci* 49:522–527
 48. Ferrara N (2004) Vascular endothelial growth factor: basic science and clinical progress. *Endocr Rev* 25:581–611
 49. Akeson A, Herman A, Wiginton D, Greenberg J (2010) Endothelial cell activation in a VEGF-A gradient: relevance to cell fate decisions. *Microvasc Res* 80:65–74
 50. Finley SD, Engel-Stefanini MO, Imoukhuede PI, Popel AS (2011) Pharmacokinetics and pharmacodynamics of VEGF-neutralizing antibodies. *BMC Syst Biol* 5:193

51. Santora LC, Kaymakcalan Z, Sakorafas P, Krull IS, Grant K (2001) Characterization of noncovalent complexes of recombinant human monoclonal antibody and antigen using cation exchange, size exclusion chromatography, and BIAcore. *Anal Biochem* 299:119–129
52. Leal T, Robins HI (2010) Bevacizumab induced reversible thrombocytopenia in a patient with recurrent high-grade glioma: a case report. *Cancer Chemother Pharmacol* 65:399–401
53. Kumar J, Bhargava M, Aggarwal S (2012) Bevacizumab-induced reversible thrombocytopenia in a patient with adenocarcinoma of colon: rare adverse effect of bevacizumab. *Case Rep Oncol Med* 2012:695430
54. Van Walle I, Gansemans Y, Parren PW, Stas P, Lasters I (2007) Immunogenicity screening in protein drug development. *Expert Opin Biol Ther* 7:405–418
55. Breustedt DA, Schönfeld DL, Skerra A (2006) Comparative ligand-binding analysis of ten human lipocalins. *Biochim Biophys Acta* 1764:161–173
56. Schlehuber S, Beste G, Skerra A (2000) A novel type of receptor protein, based on the lipocalin scaffold, with specificity for digoxigenin. *J Mol Biol* 297:1105–1120
57. Kim HJ, Eichinger A, Skerra A (2009) High-affinity recognition of lanthanide(III) chelate complexes by a reprogrammed human lipocalin 2. *J Am Chem Soc* 131:3565–3576
58. Skerra A (1994) Use of the tetracycline promoter for the tightly regulated production of a murine antibody fragment in *Escherichia coli*. *Gene* 151:131–135
59. Miles AA, Miles EM (1952) Vascular reactions to histamine, histamine-liberator and leukotaxine in the skin of guinea-pigs. *J Physiol* 118:228–257
60. Simpson-Herren L, Lloyd HH (1970) Kinetic parameters and growth curves for experimental tumor systems. *Cancer Chemother Rep* 54:143–174